C.1.c.1.23-NiAl-layered double hydroxide intercalated with.pdf

By Risfidian Mohadi

NiAl-layered double hydroxide intercalated with Keggin polyoxometalate as adsorbent of malachite green: kinetic and equilibrium studies

N. R. Palapa, T. Taher, R. Mohadi, A. Rachmat, M. Mardiyanto, M. Miksusanti & A. Lesbani

Published online: 06 Mar 2021.

Submit your article to this journal ⬀

Article views: 42

View related articles ⬀

View Crossmark data ⬀

Taylor & Francis
Taylor & Francis Group

Check for updates

NiAl-layered double hydroxide intercalated with Keggin polyoxometalate as adsorbent of malachite green: kinetic and equilibrium studies

N. R. Palapa[a], T. Taher[b], R. Mohadi[c], A. Rachmat[a], M. Mardiyanto[d], M. Miksusanti[a], and A. Lesbani[a,c]

[a]Graduate School of Mathematics and Natural Sciences Faculty, Sriwijaya University, Ogan Ilir, South Sumatra, Indonesia; [b]Department of Environmental Engineering, Inst Teknologi Sumatera, Jalan Terusan Ryacudu, Way Hui, Kecamatan Jati Agung, Lampung Selatan 35365;[c]Research Center of Inorganic Materials and Coordination Complexes, Faculty of Mathematics and Natural Sciences, Universitas Sriwijaya, Ogan Ilir, Indonesia; [d]Department of Pharmacy, Faculty of Mathematics and Natural Sciences, Sriwijaya University, Ogan Ilir, South Sumatra, Indonesia

ABSTRACT

In this study, we attempted to intercalate the Keggin polyoxometalate (POM) anion $SiW_{12}O_{40}^{4-}$ with NiAl-layered double hydroxide using a facile ion-exchange technique under a N_2 atmosphere. The obtained solids were characterized via X-ray diffraction analysis, Fourier-transform infrared spectroscopy, N_2 adsorption-desorption isotherms, scanning and transmission electron microscopes to evaluate their surface morphology. Furthermore, the synthesized materials were employed as novel adsorbents for the removal of malachite green (MG) dye from aqueous solutions. The intercalation was successful. The synthesized material as an adsorbent for the removal of MG can be used for the removal of cationic dyes from aqueous solutions. The adsorption kinetics study showed that the adsorption of MG onto NiAl-POM best fitted the pseudo-second-order model, which indicated that the adsorption process was conducted chemically. Moreover, the adsorption isotherm revealed that the adsorption occurred in a monolayer system. The regeneration process showed that the high effectivity adsorption process after fifth cycles adsorption for NiAl-POM.

Introduction

In recent decades, water-pollution issues have increased exponentially and there has been a worldwide concern to assess the quality of water resources (Schwarzenbach et al. 2010; Huang et al. 2019). Many national environmental agencies have issued regulations to maintain water-resource sustainability from various toxic and hazardous pollutants, such as dye effluents (Vikrant et al. 2018). Wastewater contains numerous pollutants that are detrimental to the environment. Dyes typically consist of complex aromatic structures that are hardly degraded in the environment. Moreover, dyes cause acute allergic, toxic, and carcinogenic responses to living organisms, including humans (Shi et al. 2014). The massive production of synthetic dyes of up to 7×10^5 tons annually, rapidly increases the amount of dye effluents discharged to the

hydrosphere (Yagub et al. 2014). Therefore, considering the safety and sustainability of water resources, an effort to remove dyes from wastewater is tremendously desired and needed.

To date, numerous endeavors have investigated the most effective way to eliminate the dye content in wastewater. Some of the most researched methods are chemical coagulation, bioremediation, chemical oxidation, photodegradation, membrane separation, and adsorption (B. Zhang et al. 2017). However, adsorption is the most deliberated technique for the treatment of contaminated wastewater owing to its easy operation, low cost, high selectivity, and high removal efficiency (Y. G. Chen et al. 2011). Moreover, the abundance of adsorbent materials that have satisfactory adsorption capacity significantly increases the selectivity and effectiveness of the adsorption process. Various adsorbents prepared with inexpensive materials have high adsorption capacities

against dye molecules, such as bentonite and layered double hydroxides (LDHs) (H. Zhang et al. 2018; Taher et al. 2019).

LDHs, also known as hydrotalcite-like materials, belong to the class of ionic lamellar compounds with a two-dimensional structure. These compounds exhibit a wide range of chemical compositions with the general formula of $[M_{1-x}^{2+}M_x^{3+}(OH)_2]^{x+}[A_{x/n}^{n-} \cdot yH_2O]^{x-}$, where M^{2+} and M^{3+} are divalent and trivalent metal cations, respectively, and A^{n-} is the n-valent anion that lies in the interlayer gallery of the LDH structure (Chubar et al. 2017). Pourfaraj et al. investigated the capability of MgAl-LDH with nanoplatelets to act as an adsorbent of brilliant yellow (BY) dye. The synthesized material exhibited a high adsorption capacity against the BY dye of up to 115 mg/g. Moreover, LDHs adsorb various anionic dyes through ion-exchange mechanisms and electrostatic interactions due to their positively charged surface. Unfortunately, these properties impede the adsorption capability of LDHs toward cationic dyes owing to electrostatic repulsions. Therefore, it is necessary to improve the capability of LDHs to adsorb both cationic and anionic dyes because industrial wastewater commonly consists of various types of dyes.

To compensate for the positively charged LDHs, anionic species such as CO_3^{2-} and NO_3^- are linked via electrostatic forces and hydrogen bonding with the hydroxyl group of the layer (Peng et al. 2015). LDHs exhibit a flexible confined space that can be adjusted by changing the interlayer anion species related to their molecular size, structure, and functionality through intercalation. By intercalating larger anionic species, the fundamental properties of LDHs, including their adsorption capability, can be significantly improved. For instance, Villegas et al. (2002) reported that manganese oxide intercalated with MgAl-LDH showed higher basal spacing and surface area than the initial LDH. Among the available anion species that can be intercalated with LDH, polyoxometalate (POM)-based anions have attracted wide interest owing to their high thermal stability, good solubility, and large molecular structure (Yun and Pinnavaia 1996).

In this study, we attempted to intercalate the Keggin-type POM anion $\alpha\text{-SiW}_{12}O_{40}^{4-}$ with NiAl-LDH and fabricate a novel material for the adsorptive removal of the cationic dye malachite green (MG), which is widely used in various industries including the textile industry. The prepared materials were characterized with respect to their crystallinity, functional groups, and surface morphologies. Additionally, we systematically investigated the effect of contact time, initial pH, initial concentration, and temperature on the adsorption behavior of MG onto the prepared materials. To the best of our knowledge, POM intercalated with NiAl LDH has not been reported for the adsorptive removal of MG dye, and we expected that the prepared material could be effective in the removal of dyes from wastewater.

Experimental section

Materials

Aluminum nitrate nonahydrate ($Al(NO_3)_3 \cdot 9H_2O$), nickel nitrate hexahydrate ($Ni(NO_3)_2 \cdot 6H_2O$), sodium carbonate (Na_2CO_3), sodium tungstate ($Na_2WO_4 \cdot 2H_2O$), and sodium metasilicate (Na_2SiO_3) were purchased from Merck. Hydrochloric acid and MG were purchased from Sigma Aldrich. All chemicals were of analytical grade and used as received without further purification.

Methods

Preparation of NiAl-LDH

In this work, the original material NiAl-LDH was prepared via a facile co-precipitation method, as previously reported by Kubo et al. (2012) Briefly, $Ni(NO_3)_2 \cdot 6H_2O$ and $Al(NO_3)_3 \cdot 9H_2O$ with a Ni:Al molar ratio of 3:1 were dissolved in deionized water. In a flask, 0.3 M Na_2CO_3 solution was prepared, and the prepared mixed metal salt solution was added dropwise into it under vigorous stirring at 80 °C. The pH of the reaction mixture was adjusted to 10 via the addition of 2 M NaOH solution, and the mixture was aged at 80 °C for 17 h. After completion, the obtained green precipitate was separated via vacuum filtration, washed with distilled water three times, and dried in an oven at 80 °C overnight. The obtained

green solid powder was then labeled as NiAl-LDH.

Preparation of NiAl-POM

The Keggin POM anion (α-SiW$_{12}$O$_{40}^{4-}$) was prepared according to our previous report Lesbani et al. (2015). The intercalation of the POM anion was conducted via a simple ion-exchange procedure as reported by Wu et al. (2018). Specifically, 1 g of NiAl-LDH was dispersed in 50 mL of distilled water at 60 °C for 6 h until a slurry solution was obtained. Subsequently, 50 mL of the POM anion solution (0.02 M) was added to the NiAl-LDH slurry under vigorous stirring. The whole process was conducted under a N$_2$ atmosphere, and the mixture was further stirred at 60 °C for 24 h. After completion, the resulting product was filtered and washed with distilled water three times, followed by drying at 80 °C overnight. The final product was labeled as NiAl-POM.

Characterization of materials

The crystallinity of the synthesized materials was evaluated via XRD analysis on a Rigaku Miniflex 600 diffractometer (Rigaku, Japan) using CuKα irradiation operating at 40 kV and 40 mA, and the data were recorded in the range of 5° to 70°. Fourier-transform infrared (FT-IR) spectroscopy was conducted with a Shimadzu Prestige-21 instrument (Shimadzu, Japan) using the KBr pellet method, and the spectra were recorded at a wavenumber of 4000–400 cm^{-1}. The surface morphology of the prepared materials was evaluated via the analysis of the N$_2$ adsorption-desorption isotherms, which was conducted using the Micromeritics ASAP 2020 surface area analyzer; the specific surface area of the sample was determined via the Brunauer-Emmett-Teller (BET) method.

Determination of pH$_{pzc}$

The point zero charge (pH$_{pzc}$) of a material is the pH at which the total negative and positive charges on the surface are equal (zero net charges). In this experiment, the pH$_{pzc}$ of the prepared samples was determined using the batch equilibrium method of Berber-Villamar et al. (2018). Typically, the prepared samples (1 g/L) were mixed with 0.1 M NaCl, adjusted previously to the initial pH (pH$_i$) of 2 to 12 via the addition of 0.1 M H$_2$SO$_4$ and 0.1 M NaOH. The mixtures were stirred continuously at room temperature for 24 h to ensure that the mixture reached equilibrium. After completion, the mixture was separated via filtration, and the final pH (pH$_f$) of each solution was measured. The graph of ΔpH (pH$_i$-pH$_f$) was plotted against the initial pH to determine the pH$_{pzc}$.

Adsorption study

The adsorption experiments were conducted using a batch technique under constant stirring at 150 rpm. Typically, 0.05 g of the prepared material contacted 50 mL of an MG solution that was previously prepared in different concentrations. The adsorption process was conducted at different time intervals, initial pH, and temperatures. The remaining concentration of MG after adsorption was determined using a UV-Vis spectrometer (Biobase, China) under the MG maximum wavelength (617 nm) (Qu et al. 2019). The adsorption capacity of each tested material against MG was calculated based on the change in the concentration of MG before and after the adsorption using the following equation:

$$q_e = \frac{(C_o - C_e)}{m} \cdot V \qquad (1)$$

where q_e is the adsorption capacity of the tested adsorbent at equilibrium (mg/g), C_o and C_e are the initial and equilibrium concentrations of the MG solutions, respectively, (mg/L), m is the amount of adsorbent used (g), and V is the volume of the MG solution (L).

Results and discussion

Characterization of adsorbents

NiAl-layered double hydroxides (LDH) were successfully prepared via the coprecipitation method, leading to the formation of NiAl-LDH with CO$_3^{2-}$/NO$_3^{-}$ interlayer anions. The Keggin POM SiW$_{12}$O$_{40}^{4-}$ was intercalated with the as-synthesized NiAl-LDH via ion exchange. The XRD pattern of the synthesized NiAl-LDH displayed in Figure 1 showed a typical reflection of the layered LDH phase at 11.83°, 23.53°, 35.29°, and 61.37° corresponding to the (003), (006), (012), and
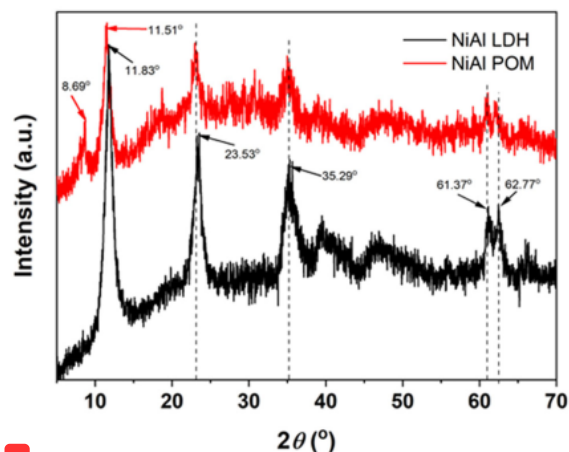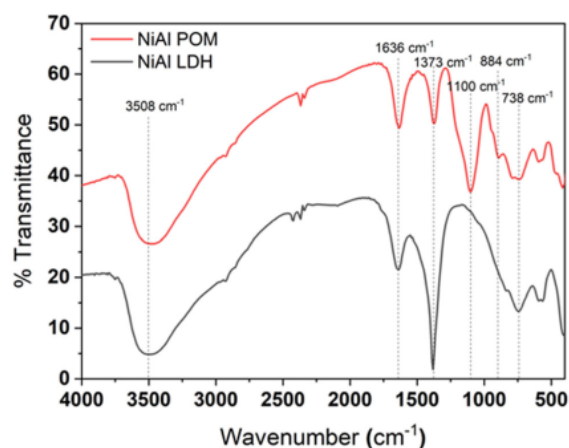
Figure 1. XRD pattern of NiAl LDH and NiAl-POM.

Figure 2. FTIR spectra of NiAl LDH and NiAl-POM.

Figure 3. FTIR spectra of NiAl LDH and NiAl-POM after MG adsorbed.

(113) basal planes, respectively (Z. Liu and Zhang 2009; Sun et al. 2019). The crystal cell parameter of the sample was calculated based on these values, and the values of a and c were 0.30 nm and 2.24 nm, respectively. The d-spacing of NiAl-LDH that corresponded to the (003) plane was 0.769 nm. This value was very close to that previously reported by Kubo et al. (2012). After intercalation with $SiW_{12}O_{40}^{4-}$, the XRD pattern of NiAl-POM exhibited a slight difference. The (003) plane, which corresponded to the basal spacing of LDH, shifted to a lower angle (8.69°), indicating the expansion of the interlayer space due to the insertion of $SiW_{12}O_{40}^{4-}$ (J. Chen 2011).

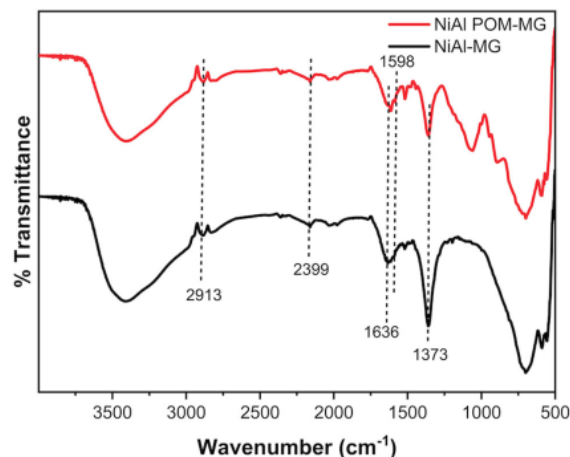The FT-IR spectra of the prepared NiAl-LDH and NiAl-POM are presented in Figure 2. The

spectrum of NiAl-LDH showed two prominent vibration bands at 3508 cm^{-1} and 1635 cm^{-1}, which corresponded to the O–H stretching and bending vibration modes of the interlayer water molecule, respectively (Carriazo et al. 2007). The remarkable peak in the spectrum of the original NiAl LDH at 1373 cm^{-1}, which corresponded to the vibration of CO_3^{2-}, was drastically reduced after intercalation with POM. Although this peak disappeared, this finding suggests that the original interlayer anion of NiAl LDH, CO_3^{2-}, was successfully replaced by the POM anion (K. Liu et al. 2016). A strong band in the spectrum of NiAl-POM at 1100 cm^{-1} was related to the vibration band of the Si–O bond. Moreover, a new weak vibration band was observed at 884 cm^{-1} and was assigned to the vibration of the W–O–W bond (J. Chen 2011). These results further indicated the presence of $SiW_{12}O_{40}^{4-}$ in the interlayer space of NiAl-LDH.

After the adsorption process, NiAl-POM and NiAl LDH were characterized using FTIR to determine the changing structure after adsorbing MG in watery phases. The FTIR spectra were shown in Figure 3, Figure 3 showed that the specific peaks of MG are showed in 1598 cm^{-1} correspond to the benzene rings (C=C bonds) from MG structure. The C-N bond is presented at 2913 cm^{-1}. Thus, another peak at 2399 cm^{-1} corresponds to the tertiary amine vibration.

The as-synthesized samples of NiAl LDH and NiAl POM have subjected to N_2 adsorption-
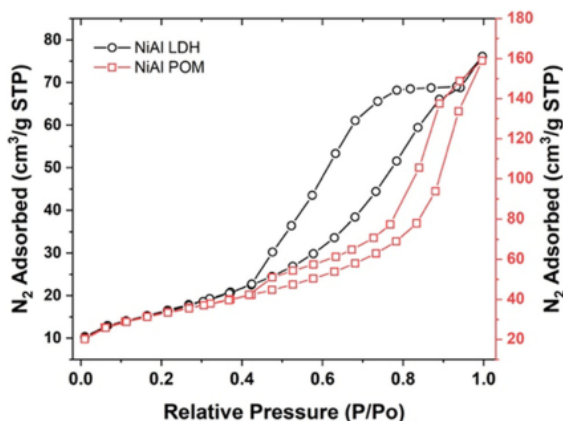
Figure 4. N$_2$ adsorption-desorption isotherm of NiAl LDH and NiAl-POM.

Table 1. Textural properties of pristine NiAl-LDH and NiAl-POM.

Properties	Sample	
	NiAl-LDH	NiAl-POM
BET surface area (m^2/g)	58.11	116.16
Total pore volume (cm^3/g)	0.117	0.245
Micropore volume (cm^3/g)	0.000413	0.006971
Average pore width (nm)	8.101	8.469

desorption analysis in order to investigate their textural properties. Figure 4 shows the N$_2$ adsorption-desorption pattern of the tested materials. Both materials showed a similar Type IV isotherm pattern but with slightly different hysteresis patterns according to the IUPAC classification, suggesting that the materials have mesoporous properties. NiAl LDH exhibited H2(a) hysteresis loop while NiAl POM showed H2(b) hysteresis type. These results indicated that the materials showed a pore-blocking with different pore-neck size in which NiAl POM with H2(a) hysteresis loop showed a much larger size distribution of neck widths. This phenomenon was assumed to be influenced by the intercalation of the SiW$_{12}$O$_{40}$$^{4-}$. The other textural properties of the tested materials are summarized in Table 1. In accordance with the previous discussion, after intercalated by SiW$_{12}$O$_{40}$$^{4-}$, the specific surface area of NiAl POM elevated in almost doubled as well as its pore volume also increased significantly. As also reported by Li et al. (2017), the increase of the LDH surface area was affected by the incorporation of the larger size anion into the interlayer space.

The physical characterization was determined using SEM and TEM characterization. The SEM images of NiAl LDH and NiAl-POM were showed in Figure 5. The SEM images of NiAl LDH and NiAl-POM showed the agglomeration which unique morphologies of LDH. According to J. Liu et al. (2014), LDH was synthesized using co-precipitation in pH 10, observed the aggregate

and irregular structure. Thus, TEM used to study the morphology of NiAl LDH and NiAl-POM (Figure 6). The darker color displays the distribution of particle due to the oppositely charged surface. The particle size of NiAl LDH and NiAl-POM was determined using ImageJ software (Kumar and Ghosh 2019). According these figures and histograms, the particle size of NiAl-POM is a uniform particle size with nanoparticle scale. However, TEM images and histogram of NiAl LDH showed the average of particle size is 1.9 nm. This finding shows the aggregate affected un-uniform morphology of NiAl LDH.

In this work, the adsorptive behavior of the synthesized NiAl-POM against the cationic MG dye was further investigated. First, the adsorption of MG was conducted at different solution pH values ranging from 4 to 8 because the adsorption depended highly on pH. As shown in Figure 7(a), the removal of MG by NiAl-POM was more favorable under alkaline conditions. To describe this phenomenon, we conducted an analysis of the pH$_{pzc}$, and that of NiAl-POM was 7.6 Figure 7(b). Based on this result, the charge of NiAl-POM at different pH solutions is illustrated in Figure 6. This result was in agreement with that of a previous study by De Sá et al. (2013), where the pH$_{pzc}$ of CaAl-LDH was 7.29. However, the researchers reported that the optimum adsorption conditions of sunset yellow dye on CaAl-LDH were acidic, which contradicted the findings of this work. The optimum conditions may be affected by the type of dye used. The MG dye was dissolved in an aqueous solution and its tri-arylmethane group was dissociated (D–N(CH$_3$)$_2$$^+$ + Cl$^-$). The surface of NiAl-LDH was positively charged below pH$_{pzc}$, so the dissociated MG dye was repulsed. Otherwise, the dissociated MG would be strongly attracted to the surface of the adsorbent because it would be negatively charged.
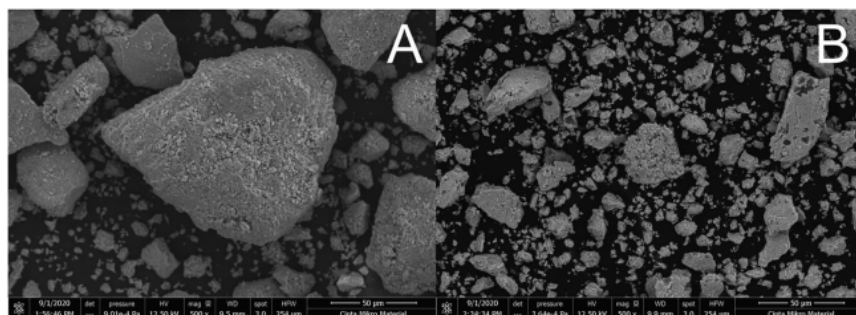
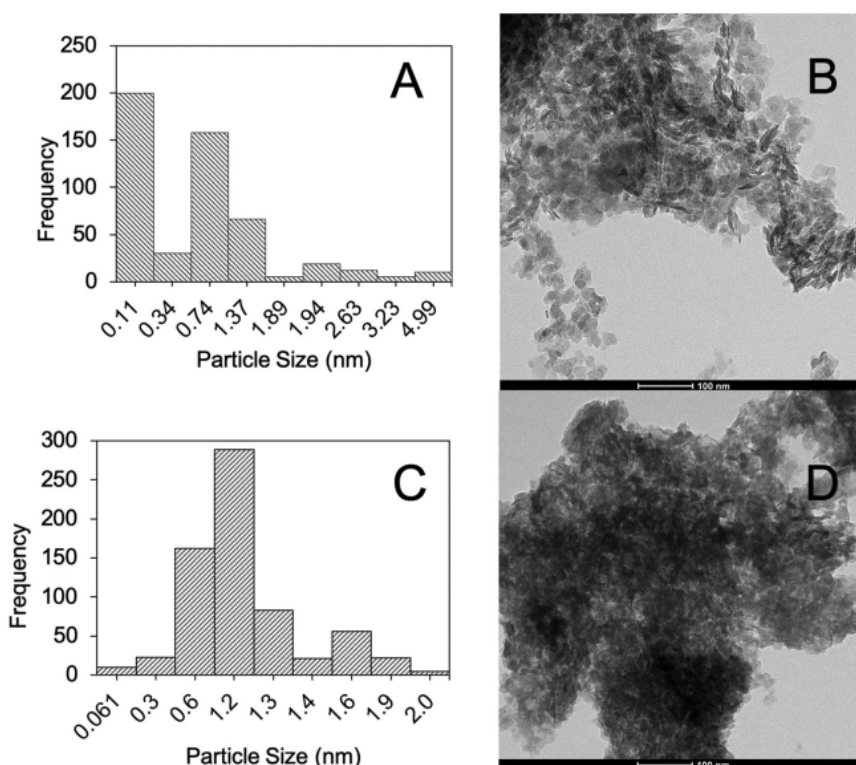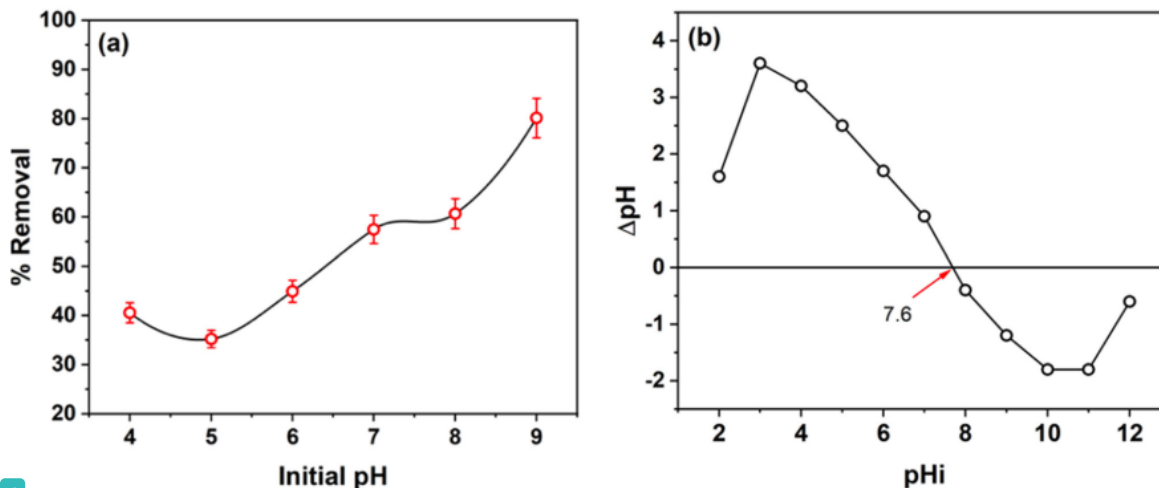**Figure 5.** SEM images of NiAl LDH (A) and NiAl-POM (B).

Figure 6. Particle size distribution histograms and TEM images of NiAl LDH (A, B) and NiAl-POM (C, D).

The effect of solution pH on surface charge of NiAl-POM was presents in Figure 8.

Next, the effect of contact time between the MG solution and the NiAl-POM adsorbent was investigated. As shown in Figure 9, the adsorption process was significantly affected by the contact time. The MG removal efficiency gradually increased with an increasing contact time, eventually reaching its maximum adsorption capacity after approximately 120 min. In the equilibrium state, the MG molecule in the solution could be removed by up to 94.09% with an equilibrium adsorption capacity of 9.42 mg/g. Moreover, the adsorption was rapid in the first 20 min. Afterwards, the adsorption proceeded slowly before reaching the equilibrium time. As reported by Berber-Villamar et al. (2018), this phenomenon was caused by (1) the availability of the binding sites for adsorption and (2) the high driving force that occurred in the initial contact time to move the dye molecule from the solution to the surface of the adsorbent.

The kinetics of the MG adsorption onto NiAl-POM was determined using the two most studied

Figure 7. Effect of initial pH on MG removal efficiency and pHpzc of the adsorbent.
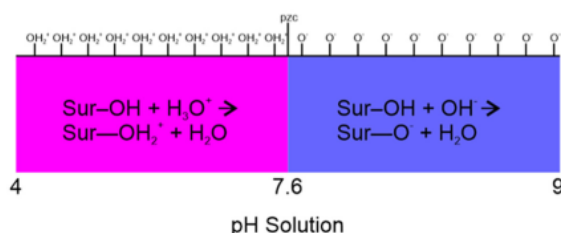

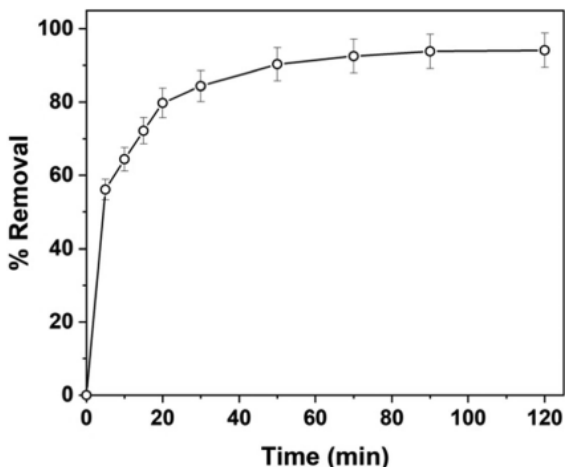**Figure 8.** Effect of pH solution on the surface charge of NiAl-POM.

Figure 9. Effect of contact time on MG removal efficiency.

kinetics models, i.e., the pseudo-first-order and pseudo-second-order models. This investigation was conducted to examine the mechanism that controls the adsorption process, including mass transfer, chemical reaction, or diffusion (Doğan and Alkan 2003). The mathematical equations of
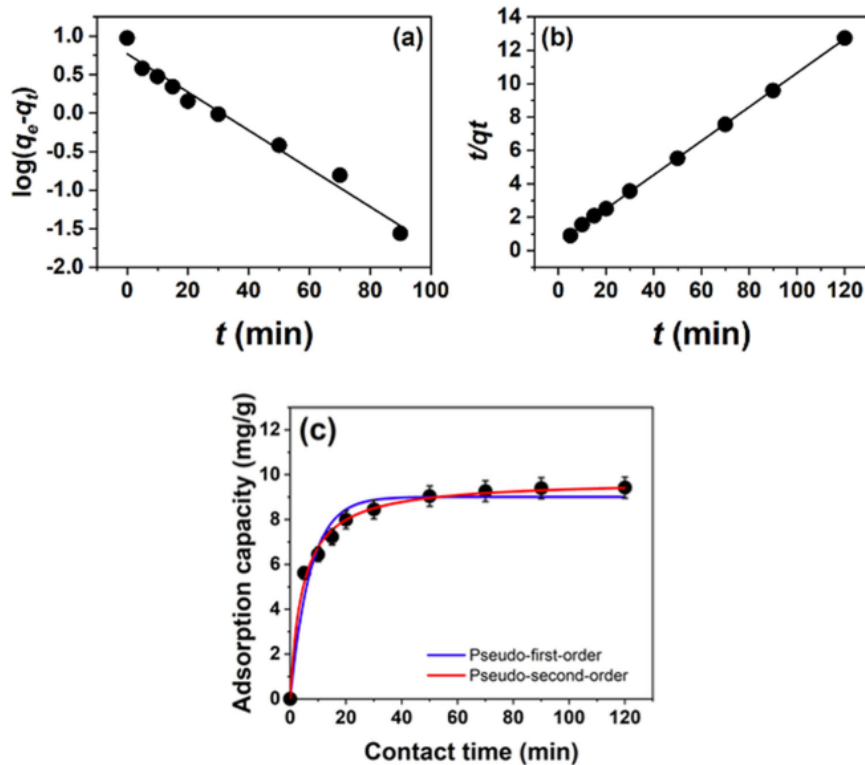
both kinetic models are presented in Table 2. The kinetic parameters of the predicted q_e and k_1 and k_2 were calculated from the intercept and slope values of these linear equations.

The linear plot of the employed model, as well as the fitted model against the experimental data, are presented in Figure 10, and the calculated kinetic parameters of the MG adsorption are presented in Table 3. Both models exhibited good linear regression against the experimental data. However, the pseudo-second-order model showed a much better correlation coefficient (R^2) that was very close to unity. The predicted adsorption capacity of the adsorbent based on the pseudo-second-order model was also much closer to the experimental value as well as the graph of the fitting model against the experimental data, as can be seen in Figure 10(c). These findings suggested that the adsorption of MG onto NiAl-POM was well described and followed the pseudo-second-order model. Based on this result, the adsorption process was possibly mainly governed by chemical interactions or chemisorption (Crini et al. 2007). Similar phenomena have also been reported for the adsorption of MG onto other adsorbents such as cyclodextrin (Crini et al. 2007), chemically modified rice husk (Bekçi et al. 2008), and bentonite (Bulut et al. 2008).

The adsorption isotherm equilibrium was investigated at different initial MG concentrations. The adsorption isotherm of MG into

Table 2. Mathematical equation of the employed kinetic models.

Pseudo-first order (PFO)	Nomenclature
$\log(q_e - q_t) = \log q_e - \frac{k_1}{2.303} \cdot t$ Pseudo-second order (PSO) $\frac{t}{q_t} = \frac{1}{k_2 q_e^2} + \frac{1}{q_e} \cdot t$	• q_e = equilibrium adsorption capacity (mg/g) • q_t = adsorption capacity at certain time (mg/g) • k_1 = rate constant of the PFO model (1/h) • k_2 = rate constant of the PSO model (1/h)

Figure 10. Plots of pseudo-first-order (a) and pseudo-second-order (b) kinetic models, and fitted model against experimental data (c).

Table 3. Kinetic parameters of MG adsorption onto NiAl-POM.

Pseudo-first order	Value	Pseudo-second order	Value
k_1 (1/min)	0.0571	k_2 (g/mg min)	0.0218
$q_{e,cal}$ (mg/g)	5.8712	$q_{e,cal}$ (mg/g)	9.8321
R^2	0.9787	R^2	0.9998

NiAl-POM at temperatures ranging from 30 °C to 50 °C is shown in Figure 11. The adsorption capacity, q_e, gradually increased with an increasing initial concentration of MG, as previously reported Tang et al. (2012). For further investigation of the adsorption, two adsorption isotherm models, i.e., the Langmuir and Freundlich's isotherms, were applied to the obtained experimental data. The Langmuir isotherm model was designed to describe the
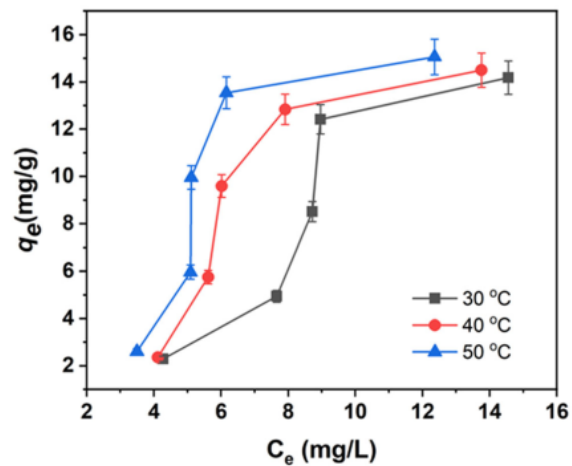

Figure 11. Adsorption isotherm of MG onto NiAl-POM at different temperatures.

Table 4. Comparison of MG adsorbed onto NiAl-POM and the other adsorbents.

Adsorbents	Higher adsorption capacity (mg/g)	Dosage (mg)	Initial concentration (mg/L)	References
Humic acid	6	20	5–300	Lee et al. (2019)
RH-Biochar	31.4	250	100	Palapa et al. (2020b)
ADR-activated carbon	9	100	100	J. Zhang et al. (2008)
Rice husk	12	100	100	Chowdhury et al. (2011)
zeolite	24	30	160	Han et al. (2010)
NiFe LDH	5.23	250	25	Lesbani et al. (2020)
Bentonite	179	100	300	Bulut et al. (2008)
FeFe2O3@PDA	66.9	100	100	Wang et al. (2018)
NiFe-SiW$_{12}$O$_{40}$	8.81	50	50	Lesbani et al. (2020)
Bentonite/Co$_3$O$_4$	343	50	100	Abdel Salam et al. (2020)
Co/ZnO algae	5	20	10	Rabie et al. (2020)
Xerogel-activated	4.2	90	10	Sriram et al. (2019)
CuAl LDH	55.8	50	100	Palapa et al. 2020a)
Waste paper activated carbon	23	250	25	(Méndez et al. 2007)
Diatomite@Ni/NiO	47	50	25	(G. Liu et al. 2020)
NiAl-POM	7.84	50	12	This work

Table 5. Isotherm parameters of MG adsorption onto NiAl POM.

Adsorption temperature	Langmuir			Freundlich		
	q_{max}	b	R^2	K_f	n	R^2
30 °C	7.4519	0.0560	0.9394	0.2495	0.6311	0.8645
40 °C	6.5588	0.0743	0.7626	0.5126	0.7164	0.7293
50 °C	7.8490	0.0821	0.7478	0.8538	0.7932	0.6626

monolayer adsorption that occurred on the homogenous surface. This model is presented in the following equation (Annadurai et al. 2002; Foo and Hameed 2010):

$$\frac{1}{q_e} = \frac{1}{q_{max}} + \frac{1}{q_{max}b} \cdot \frac{1}{C_e} \quad (2)$$

where q_{max} is the maximum adsorption capacity of the monolayer (mg/g), b is the Langmuir adsorption equilibrium constant (1/mg), and C_e is the equilibrium concentration of MG (mg/L). The isotherm parameter based on the Langmuir model was determined from the slope and intercept values of the $1/q_e$ versus $1/C_e$ plot.

Next, the Freundlich adsorption isotherm model was employed. This model was used to describe an adsorption phenomenon that occurred on a heterogeneous surface in which the adsorption capacity is related to the concentration of the dye (Kushwaha et al. 2014). The linear form of the Freundlich model can be written as follows (Allen et al. 2004):

$$\ln q_e = \ln K_f + \left(\frac{1}{n}\right)\ln C_e \quad (3)$$

where K_f and n are the Freundlich constants

corresponding to the adsorption capacity and adsorption intensity, respectively. These parameters can be calculated from the slope and intercept values of the plot of $\ln q_e$ against $\ln C_e$. The maximum adsorption capacity of MG by NiAl-POM was compared to the other adsorbents, which have previously been reported. The comparison results were listed in Table 4. The amount of MG adsorbed by several materials with different treatment of adsorption. However, the higher adsorption capacity of MG is difficult to compare the amount of MG removal of several adsorbents due to different initial concentration, dosages of adsorbent, pH condition and temperature adsorption. In addition, the higher adsorption capacity using NiAl-POM is 7.84 mg/g from initial concentration 12 mg/L. Thus, the intercalation process using POM onto LDH has removal percentage 65.33%.

The adsorption isotherm parameters of MG onto the NiAl-POM adsorbent are presented in Table 5. Based on the value of the regression coefficient (R^2), the adsorption mechanism was best described by the Langmuir model. Thus, the adsorption was conducted on the monolayer surface, as also reported by Tang et al. (2012). Moreover, this finding was in accordance with the predicted kinetics model, which assumed that the adsorption process was conducted chemically.

Furthermore, the regeneration process is important for the practical uses of adsorbent. The reusability process was carried out to determine the effectivity of adsorbent's modification uses.
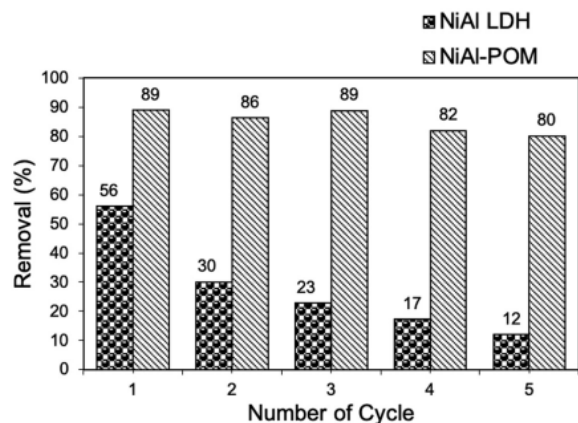
Figure 12. Regeneration efficiency of NiAl LDH and NiAl-POM.

To regenerate NiAl-POM, the adsorbed material was prepared to desorb using water by ultrasonic bath Delta D68H for 30 minutes. As presented data in Figure 12, after fifth cycles, the efficiency for MG removal onto NiAl-POM was decreases from 89% to 80.2%, and 56% to 12% for NiAl LDH. These findings showed the good regeneration of NiAl-POM than NiAl LDH. According to Momina et al. (2019) the regeneration process which adopted ultrasonic treatment is depended on the adsorbent and adsorbate types. This technique is effective to remove the dye molecule from layer stacked on LDH or modified LDH.

Conclusions

NiAl-LDH was successfully synthesized via a facile coprecipitation method under alkaline conditions. Further modification of the synthesized NiAl-LDH was successfully performed by intercalating the POM anion $SiW_{12}O_{40}^{4-}$ with NiAl-LDH. The success of the intercalation was confirmed by the increase in the interlayer space or interlayer gallery, as well as by the significant decrease in the number of original anion species of NiAl-LDH. The synthesized NiAl-POM as an adsorbent for the removal of MG showed good potential for the removal of cationic dyes, even, after fifth regeneration.

Acknowledgements

References

Abdel Salam M, Abukhadra MR, Adlii A. 2020. Insight into the adsorption and photocatalytic behaviors of an organo-bentonite/Co3O4 green nanocomposite for malachite green synthetic dye and Cr(VI) metal ions: application and mechanisms. ACS Omega. 5(6):2766–2778. doi:10.1021/acsomega.9b03411

Allen SJ, Mckay G, Porter JF. 2004. Adsorption isotherm models for basic dye adsorption by peat in single and binary component systems. J Colloid Interface Sci. 280(2):322–333. doi:10.1016/j.jcis.2004.08.078

Annadurai G, Juang RS, Lee DJ. 2002. Use of cellulose-based wastes for adsorption of dyes from aqueous solutions. J Hazard Mater. 92(3):263–274. doi:10.1016/S0304-3894(02)00017-1

Bekçi Z, Özveri C, Seki Y, Yurdakoç K. 2008. Sorption of malachite green on chitosan bead. J Hazard Mater. 154(1–3):254–261. doi:10.1016/j.jhazmat.2007.10.021

Berber-Villamar NK, Netzahuatl-Muñoz AR, Morales-Barrera L, Chávez-Camarillo GM, Flores-Ortiz CM, Cristiani-Urbina E. 2018. Corncob as an effective, eco-friendly, and economic biosorbent for removing the azo dye Direct Yellow 27 from aqueous solutions. PLoS One. 13(4):e0196428–30. doi:10.1371/journal.pone.0196428

Bulut E, Özacar M, Şengil IA. 2008. Adsorption of malachite green onto bentonite: equilibrium and kinetic studies and process design. Microporous Mesoporous Mater. 115(3):234–246. doi:10.1016/j.micromeso.2008.01.039

Carriazo D, Lima S, Martín C, Pillinger M, Valente AA, Rives V. 2007. Metatungstate and tungstoniobate-containing LDHs: preparation, characterisation and activity in epoxidation of cyclooctene. J Phys Chem Solids. 68(10):1872–1880. doi:10.1016/j.jpcs.2007.05.012

Chen J. 2011. Host-guest functional materials. In: Modern inorganic synthetic chemistry. Vol. 2. p. 405–428. Netherland: Elsevier. doi:10.1016/B978-0-444-53599-3.10018-6

Chen YG, Ye WM, Yang XM, Deng FY, He Y. 2011. Effect of contact time, pH, and ionic strength on Cd(II) adsorption from aqueous solution onto bentonite from Gaomiaozi. Environ Earth Sci. 64(2):329–336. doi:10.1007/s12665-010-0850-6

Chowdhury S, Mishra R, Saha P, Kushwaha P. 2011. Adsorption thermodynamics, kinetics and isosteric heat of adsorption of malachite green onto chemically modified rice husk. Desalination. 265(1–3):159–168. doi:10.1016/j.desal.2010.07.047

Chubar N, Gilmour R, Gerda V, Mičušík M, Omastova M, Heister K, Man P, Fraissard J, Zaitsev V. 2017. Layered double hydroxides as the next generation inorganic anion exchangers: synthetic methods versus applicability. Adv

Colloid Interface Sci. 245:62–80. doi:10.1016/j.cis.2017.04.013

Crini G, Peindy HN, Gimbert F, Robert C. 2007. Removal of C.I. Basic Green 4 (Malachite Green) from aqueous solutions by adsorption using cyclodextrin-based adsorbent: kinetic and equilibrium studies. Sep Purif Technol. 53(1):97–110. doi:10.1016/j.seppur.2006.06.018

De Sá FP, Cunha BN, Nunes LM. 2013. Effect of pH on the adsorption of Sunset Yellow FCF food dye into a layered double hydroxide (CaAl-LDH-NO3). Chem Eng J. 215–216:122–127. doi:10.1016/j.cej.2012.11.024

Doğan M, Alkan M. 2003. Adsorption kinetics of methyl violet onto perlite. Chemosphere. 50(4):517–528. doi:10.1016/S0045-6535(02)00629-X

Foo KY, Hameed BH. 2010. Insights into the modeling of adsorption isotherm systems. Chem Eng J. 156(1):2–10. doi:10.1016/j.cej.2009.09.013

Han R, Wang Y, Sun Q, Wang L, Song J, He X, Dou C. 2010. Malachite green adsorption onto natural zeolite and reuse by microwave irradiation. J Hazard Mater. 175(1–3):1056–1061. doi:10.1016/j.jhazmat.2009.10.118

Huang D, Liu C, Zhang C, Deng R, Wang R, Xue W, Luo H, Zeng G, Zhang Q, Guo X. 2019. Cr(VI) removal from aqueous solution using biochar modified with Mg/Al-layered double hydroxide intercalated with ethylenediaminetetraacetic acid. Bioresour Technol. 276(November 2018): 127–132. doi:10.1016/j.biortech.2018.12.114

Kubo D, Tadanaga K, Hayashi A, Tatsumisago M. 2012. Hydroxide ion conduction in Ni-Al layered double hydroxide. Electroanal Chem. 671(3):102–105. doi:10.1016/j.jelechem.2012.02.007

Kumar A, Ghosh SK. 2019. Size distribution analysis of wear debris generated in HEMM engine oil for reliability assessment: a statistical approach. Measurement. 131: 412–418. doi:10.1016/j.measurement.2018.09.012

Kushwaha AK, Gupta N, Chattopadhyaya MC. 2014. Removal of cationic methylene blue and malachite green dyes from aqueous solution by waste materials of Daucus carota. J Saudi Chem Soc. 18(3):200–207. doi:10.1016/j.jscs.2011.06.011

Lee S-L, Park J-H, Kim S-H, Kang S-W, Cho J-S, Jeon J-R, Lee Y-B, Seo D-C. 2019. Sorption behavior of malachite green onto pristine lignin to evaluate the possibility as a dye adsorbent by lignin. Appl Biol Chem. 62(37):1–10. doi:10.1186/s13765-019-0444-2

Lesbani A, Marpaung A, Verawaty M, Rizki Amalia H, Mohadi R. 2015. Catalytic desulfurization of benzothiophene using Keggin type polyoxometalates as catalyst. J Pure App Chem Res. 4(1):5–11. doi:10.21776/ub.jpacr.2015.004.01.202

Lesbani A, Taher T, Neza Palapa R, Mohadi R, Rachmat A, Mardiyanto SN. 2020. Preparation and utilization of Keggin-type polyoxometalate intercalated Ni-Fe layered double hydroxides for enhanced adsorptive removal of cationic dye. SN Appl Sci. 2:470. doi:10.1007/s42452-020-2300-8

Li T, Miras H, Song Y-F. 2017. Polyoxometalate (POM)-layered double hydroxides (LDH) composite materials: design and catalytic applications. Catalysts. 7(9):260. doi:10.3390/catal7090260

Liu G, Abukhadra MR, El-Sherbeeny AM, Mostafa AM, Elmeligy MA. 2020. Insight into the photocatalytic properties of diatomite@Ni/NiO composite for effective photo-degradation of malachite green dye and photo-reduction of Cr (VI) under visible light. J Environ Manage. 254(May 2019):109799. doi:10.1016/j.jenvman.2019.109799

Liu J, Li X, Luo J, Duan C, Hu H, Qian G. 2014. Enhanced decolourisation of methylene blue by LDH-bacteria aggregates with bioregeneration. Chem Eng J. 242: 187–194. doi:10.1016/j.cej.2013.10.058

Liu K, Xu Y, Yao Z, Miras HN, Song YF. 2016. Polyoxometalate-intercalated layered double hydroxides as efficient and recyclable bifunctional catalysts for cascade reactions. ChemCatChem. 8(5):929–937. doi:10.1002/cctc.201501365

Liu Z, Zhang FS. 2009. Removal of lead from water using biochars prepared from hydrothermal liquefaction of biomass. J Hazard Mater. 167(1–3):933–939. doi:10.1016/j.jhazmat.2009.01.085

Méndez A, Fernández F, Gascó G. 2007. Removal of malachite green using carbon-based adsorbents. Desalination. 206(1–3):147–153. doi:10.1016/j.desal.2006.03.564

Momina Rafatullah M, Ismail S, Ahmad A. 2019. Optimization study for the desorption of methylene blue dye from clay based adsorbent coating. Water (Switzerland). 11(6):1304. doi:10.3390/w11061304

Palapa NR, Juleanti N, Normah N, Taher T, Lesbani A. 2020a. Unique adsorption properties of malachite green on interlayer space of Cu-Al and Cu-Al-SiW12O40 layered double hydroxides. Bull Chem React Eng Catal. 15(3):653–661. doi:10.9767/bcrec.15.3.8371.653-661

Palapa NR, Taher T, Rahayu BR, Mohadi R, Rachmat A, Lesbani A. 2020b. CuAl LDH/Rice husk biochar composite for enhanced adsorptive removal of cationic dye from aqueous solution. Bull Chem React Eng Catal. 15(2): 525–537. doi:10.9767/bcrec.15.2.7828.525-537

Peng C, Dai J, Yu J, Yin J. 2015. Calcined Mg-Fe layered double hydroxide as an absorber for the removal of methyl orange. AIP Adv. 5(5):057138. doi:10.1063/1.4921455

Qu W, Yuan T, Yin G, Xu S, Zhang Q, Su H. 2019. Effect of properties of activated carbon on malachite green adsorption. Fuel. 249(February):45–53. doi:10.1016/j.fuel.2019.03.058

Rabie AM, Abukhadra MR, Rady AM, Ahmed SA, Labena A, Mohamed HSH, Betiha MA, Shim J-J. 2020. Instantaneous photocatalytic degradation of malachite green dye under visible light using novel green Co–ZnO/algae composites. Res Chem Intermed. 46(3):1955–1973. doi:10.1007/s11164-019-04074-x

Schwarzenbach RP, Egli T, Hofstetter TB, von Gunten U, Wehrli B. 2010. Global water pollution and human

health. Annu Rev Environ Resour. 35(1):109–136. doi:10.1146/annurev-environ-100809-125342

Shi H, Li W, Zhong L, Xu C. 2014. Methylene blue adsorption from aqueous solution by magnetic cellulose/graphene oxide composite: equilibrium, kinetics, and thermodynamics. Ind Eng Chem Res. 53(3):1108–1118. doi:10.1021/ie4027154

Sriram G, Uthappa UT, Kigga M, Jung HY, Altalhi T, Brahmkhatri V, Kurkuri MD. 2019. Xerogel activated diatoms as an effective hybrid adsorbent for the efficient removal of malachite green. New J Chem. 43(9): 3810–3820. doi:10.1039/C9NJ00015A

Sun X, Dong J, Li Z, Liu H, Jing X, Chi Y, Hu C. 2019. Mono-transition-metal-substituted polyoxometalate intercalated layered double hydroxides for the catalytic decontamination of sulfur mustard simulant. Dalton Trans. 48(16):5285–5291. doi:10.1039/c9dt00395a

Taher T, Rohendi D, Mohadi R, Lesbani A. 2019. Congo red dye removal from aqueous solution by acid-activated bentonite from sarolangun: kinetic, equilibrium, and thermodynamic studies. Arab J Basic Appl Sci. 26(1): 125–136. doi:10.1080/25765299.2019.1576274

Tang H, Zhou W, Zhang L. 2012. Adsorption isotherms and kinetics studies of malachite green on chitin hydrogels. J Hazard Mater. 209–210:218–225. doi:10.1016/j.jhazmat.2012.01.010

Vikrant K, Giri BS, Raza N, Roy K, Kim KH, Rai BN, Singh RS. 2018. Recent advancements in bioremediation of dye: current status and challenges. Bioresour Technol. 253(January):355–367. doi:10.1016/j.biortech.2018.01.029

Villegas JC, Giraldo OH, Suib SL. 2002. New layered double hydroxides containing intercalated manganese oxide nanoparticles: synthesis and characterization. Abstracts of Papers of the American Chemical Society. 508-INOR.224(18).

Wang K, Fu J, Wang S, Gao M, Zhu J, Wang Z, Xu Q. 2018. Polydopamine-coated magnetic nanochains as efficient dye adsorbent with good recyclability and magnetic separability. J Colloid Interface Sci. 516:263–273. doi:10.1016/j.jcis.2018.01.067

Wu X, Ci C, Du Y, Liu XZ, Li X, Xie X. 2018. Facile synthesis of NiAl-LDHs with tunable establishment of acid-base activity sites. Mater Chem Phys. 211:72–78. doi:10.1016/j.matchemphys.2018.02.015

Yagub MT, Sen TK, Afroze S, Ang HM. 2014. Dye and its removal from aqueous solution by adsorption: a review. Adv Colloid Interface Sci. 209:172–184. doi:10.1016/j.cis.2014.04.002

Yun SK, Pinnavaia TJ. 1996. Layered double hydroxides intercalated by polyoxometalate anions with Keggin, Dawson, and Finke structures. Inorg Chem. 35(23): 6853–6860. doi:10.1021/ic960287u

Zhang B, Dong Z, Sun D, Wu T, Li Y. 2017. Enhanced adsorption capacity of dyes by surfactant-modified layered double hydroxides from aqueous solution. J Ind Eng Chem. 49(2016):208–218. doi:10.1016/j.jiec.2017.01.029

Zhang H, Chen H, Azat S, Mansurov ZA, Liu X, Wang J, Su X, Wu R. 2018. Super adsorption capability of rhombic dodecahedral Ca-Al layered double oxides for Congo red removal. J Alloys Compd. 768:572–581. doi:10.1016/j.jallcom.2018.07.241

Zhang J, Li Y, Zhang C, Jing Y. 2008. Adsorption of malachite green from aqueous solution onto carbon prepared from Arundo donax root. J Hazard Mater. 150(3): 774–782. doi:10.1016/j.jhazmat.2007.05.036

C.1.c.1.23-NiAl-layered double hydroxide intercalated with.pdf

ORIGINALITY REPORT

14%

SIMILARITY INDEX

PRIMARY SOURCES

1	aip.scitation.org Internet	107 words —	2%
2	jestec.taylors.edu.my Internet	106 words —	2%
3	www.x-mol.com Internet	96 words —	2%
4	www.tandfonline.com Internet	60 words —	1%
5	www.univ-usto.dz Internet	44 words —	1%
6	www.ect-journal.kz Internet	35 words —	1%
7	www.science.gov Internet	33 words —	1%
8	tel.archives-ouvertes.fr Internet	31 words —	1%
9	eprints.lib.hokudai.ac.jp Internet	30 words —	1%